Clim Dyn (2012) 38:121–140
DOI 10.1007/s00382-011-1010-8

Large-scale circulation patterns and related rainfall in the Amazon Basin: a neuronal networks approach

Jhan Carlo Espinoza · Matthieu Lengaigne · Josyane Ronchail · Serge Janicot

Received: 23 June 2010 / Accepted: 25 January 2011 / Published online: 11 February 2011
© Springer-Verlag 2011

Abstract This study describes the main circulation patterns (CP) in the Amazonian Basin over the 1975–2002 period and their relationship with rainfall variability. CPs in the Amazonian Basin have been computed for each season from the ERA-40 daily 850 hPa winds using an approach combining artificial neural network (Self Organizing Maps) and Hierarchical Ascendant Classification. A 6 to 8 cluster solutions (depending on the season considered) is shown to yield an integrated view of the complex regional circulation variability. For austral fall, winter and spring the temporal evolution between the different CPs shows a clear tendency to describe a cycle, with southern wind anomalies and their convergence with the trade winds progressing northward from the La Plata Basin to the Amazon Basin. This sequence is strongly related to eastward moving extra tropical perturbations and their incursion toward low latitude that modulate the geopotential and winds over South America and its adjoining oceans. During Austral summer, CPs are less spatially and temporally organized compared to other seasons, principally due to weaker extra tropical perturbations and more frequent shallow low situations. Each of these CPs is shown to be associated with coherent northward moving regional rainfall patterns (both in in situ data and ERA-40 reanalysis) and convective activity. However, our results reveals that precipitation variability is better reproduced by ERA-40 in the southern part of the Amazonian Basin than in the northern part, where rainfall variability is likely to be more constrained by local and subdaily processes (e.g. squall lines) that could be misrepresented in the reanalysis dataset. This analysis clearly illustrates the existing connections between the southern and northern part of the Amazonian Basin in terms of regional circulation/rainfall patterns. The identification of these CPs provide useful information to understand local rainfall variability and could hence be used to better understand the influence of these CPs on the hydrological variability in the Amazonian Basin.

Keywords Circulation patterns · South America · Amazon Basin · Rainfall · Low level winds · Self-organizing maps

1 Introduction

The Amazon drainage basin includes the world's largest rain forest and its average discharge is the greatest in the world (209 000 m^3/s; Molinier et al. 1996). Due to its size (6 000 000 km^2), its position on both sides of the Equator (5°N to 20°S), its topography, and its two adjoining oceans, the Amazon Basin displays a wide range of surface and atmospheric conditions. As shown on Fig. 1, low level winds in this region are characterized by Northeast trade winds blowing from the tropical Atlantic deflected towards the "Chaco low" (a surface low pressure near 25°S and 65°W more prominent during austral summer) when approaching the eastern slope of the Andes Cordillera. It results in a northwestern low level flow to the East of the Andes, also called low level Jet (LLJ) when its complies with specific criteria (Bonner 1968). The region between

J. C. Espinoza (✉) · M. Lengaigne · J. Ronchail · S. Janicot
LOCEAN—IPSL (IRD, CNRS, MNHN, UPMC),
Boite 100, 4 Place Jussieu, 75252 Paris Cedex 05, France
e-mail: jhan-carlo.espinoza@locean-ipsl.upmc.fr

J. C. Espinoza
Universidad Agraria La Molina UNALM, Lima, Peru

J. Ronchail
Université Paris 7, Paris, France

Andes and the Brazilian Shield is a moisture corridor into central and southern South America (e.g. Berri and Inzunza 1993; Saulo et al. 2000). The other major climatological feature in this region during summer is the South Atlantic convergence zone (SACZ; Fig. 1a), an elongated, stationary (lasting more than 4 days), Northwest/Southeast band of nebulosity extending from the northwestern Amazon Basin into the subtropical Atlantic (e.g., Kodama 1992; Lenters and Cook 1995; Liebmann et al. 1999), forced by synoptic-scale waves from the midlatitudes (e.g., Sugahara et al. 1994; Liebmann et al. 1999). The SACZ and convective activity in the Amazon Basin are the main components of the South American monsoon system (SAMS) (Jones and Carvalho 2002; Vera et al. 2006). In austral winter, deep convection strongly weakens in the southern and central part of the Amazon Basin and increases in the extreme North as a result of SAMS retreat and the displacement of the South Atlantic anticyclone towards the continent (Fig. 1b).

Aside these seasonal modulations, the Amazonian Basin also experiences large dynamical and thermodynamical variations at subseasonal timescales (Satyamurty et al. 1998). Cross equatorial low level flow over western Amazon has been shown to be strongly related with submonthly precipitation, a southerly flow being generally associated with precipitation located north of the equator (Wang and Fu 2002). These fluctuations could be partly related to SACZ that is characterized by large spatial and temporal variability that depends on the interplay of phenomena on a broad range of scales (Carvalho et al. 2002a, 2002b). The SACZ experiences large fluctuations in the intensity of rainfall at submonthly timescales (Kiladis and Weickmann 1997; Liebmann et al. 1999, 2004; de Souza and Ambrizzi 2006) with impacts on circulation (Jones and Carvalho 2002), mesoscale activity (Petersen et al. 2002) and extreme precipitation (Carvalho et al. 2004). These fluctuations are related to eastward moving mid-latitude Rossby wave trains originating over the westerly storm track in the South Pacific (Kiladis and Weickmann 1992, Ambrizzi and Hoskins 1997). These mid-latitude waves turn towards the equator as they cross the Andes and modulate the intensity of the SACZ and the LLJ. Indeed, a strong LLJ is out of phase with intense SACZ that is associated with westerly intraseasonal anomalies of the low level circulation over central South America (Jones and Carvalho 2002; Carvalho et al. 2002a) and pronounced convective rainfall events in the southern part of the Amazon Basin (Oliveira and Nobre 1986; Nogues-Peagle and Mo 1997; Diaz and Aceituno 2003; Marengo et al. 1997).

Mid-latitude cold fronts have also been shown to modulate the day-to-day variability of deep convection and rainfall in the southern tropics (e.g. Oliveira and Nobre 1986; Montes de Oca 1995). These transient disturbances from mid-latitude modulate the convective activity in the SACZ (Lenters and Cook 1995), contributing as much as

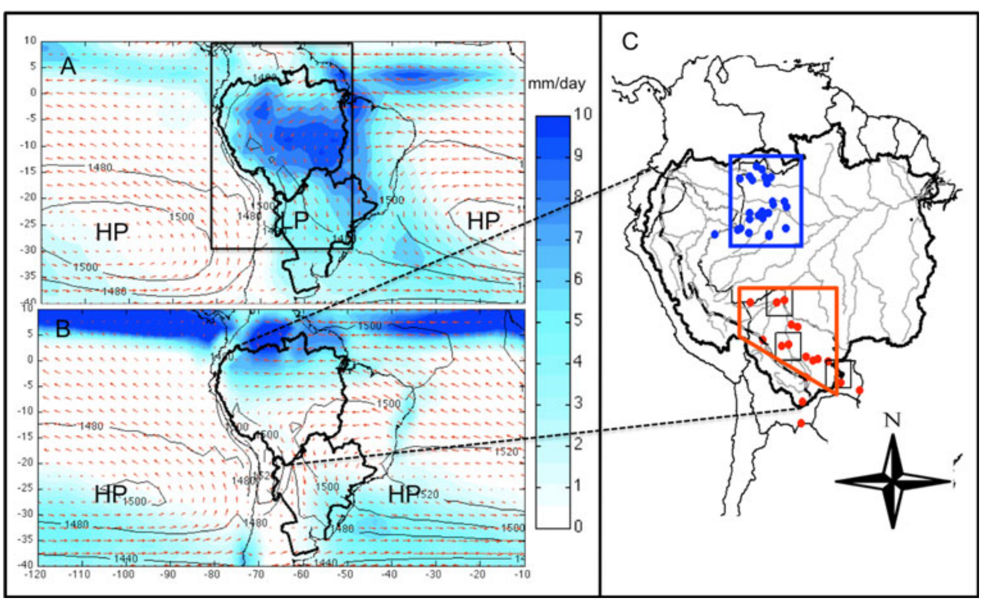

Fig. 1 Mean rainfall, geopotential height and total winds at 850 hPa for the 1967–2002 period for **a** December–January–February and **b** June–July–August. ERA-40 reanalysis data are used for geopotential and winds while rainfall monthly mean fields are computed using the Climate Prediction Center (CPC) Merged Analysis of Rainfall (CMAP) dataset (Xie and Arkin 1997) for the 1979–2002 period. **c** Limit of the Amazon Basin (*solid line*), limit of the Andean region above 500 meters (*black and white line*) and location of the rainfall gauges. *Blue and red boxes* are the limit of Northwest and South regions, respectively. The *black box* in **a**, shows the region take into account for the definition of circulation patterns (10°N–30°S and 50°W–80°W)

25% to the summertime precipitation in the central Amazonia (Garreaud and Wallace 1998). In winter, the convective activity related to cold fronts is less active but these transient disturbances occasionally generate very cold episodes leading to frost in southern Brazil (Marengo et al. 1997) and very low temperature in the Bolivian Amazon (Ronchail 1989) and their impact may be remarkable until the Columbian Amazon (Poveda et al. 2006).

Precipitation and circulation over Amazon Basin also display variability at higher frequency (typically <5 days) that can be attributed to a multitude of more local and short-lived atmospheric processes, including mesoscale convective complexes (MCC; Maddox 1980) and squall lines (Gastang et al. 1994) which have been documented using satellites or radars observations at sub-daily timescale (i.e. Cohen et al. 1995; Janowiak et al. 2005; Zipser et al. 2006; Durkee et al. 2009). MCCs are more frequent in the La Plata basin and in the South of the Amazon Basin as compared to the Northwest (Zipser et al. 2006; Durkee et al. 2009). The great majority of these convective systems occur in summer, over land; they have a short life cycle (less than a day) and they concentrate immediately downwind of the Andes (Velasco and Fritsch 1987; Laurent et al. 2002; Carvalho et al. 2002b), in an unstable atmosphere favoured by the confluence of the LLJ and the subtropical jet (Satyamurty et al. 1998; Zipser et al. 2004). Lines of instability are observed in the northern part of the Amazon Basin. They form along the northern coast of South America and propagate inland over the Amazon Basin at speeds of 50–60 km h^{-1} (Gastang et al. 1994; Greco et al. 1994). Squall lines have been suggested to occur more often when large-scale atmospheric conditions are characterized by a strong and deep low level easterly jet and a heat source in the western Amazon (Cohen et al. 1995). At mesoscale and close to the sea, an advection of moisture produced by a sea breeze is observed. At cloud scale, squall lines propagate towards the Amazon for lengths of over 1000 km and over 17 h. Janowiak et al. (2005) shows that alternating sea and land breezes during the diurnal cycle organize distinct instability lines. They penetrate farther inland in winter when the thermal gradient between the land and the ocean is greater (Planchon et al. 2006). Nocturnal convective systems in Southwestern Amazon that weaken and delay the onset of the following afternoon's convection are found to be traced to large-scale squall lines (Rickenbach 2004).

Most of the aforementioned studies discuss the relationship between some well-identified atmospheric phenomena (cold fronts, MJO, LLJ, SACZ variations, squall lines…) and circulation and/or precipitation patterns in South America at subseasonal timescales. Though, a synthetic description of the large-scale atmospheric patterns existing over the whole Amazon Basin at subseasonal timescale and of their relationship to regional rainfall has to be conducted. This can be achieved by partitioning the atmospheric states into broad categories of recurrent spatial large-scale atmospheric patterns allowing for a description of the behaviour of day-to-day motions. These circulation patterns (CPs) can often be related to some dependent local variables such as rainfall or temperature (Hewitson and Crane 2002). Clustering methods have been commonly used to define these CPs in the extra-tropics and investigate regional atmospheric variability at synoptic scales (e.g., Michelangeli et al. 1995; Fink et al. 2004). In South America, the few studies discussing CPs or weather types indeed focussed on the southern temperate regions (Solman and Menéndez 2003; Bischoff and Vargas 2003; Bettolli et al. 2010) or the Nordeste of Brazil (Chaves and Cavalcanti 2001). This approach has been recently applied in the tropics to describe the intraseasonal fluctuations of the African monsoon (Moron et al. 2008; Gueye et al. 2010) but a similar investigation in the South American tropics is still missing. The goals of this paper are therefore (i) to use an objective clustering method to identify the main large-scale atmospheric circulation patterns existing over the Amazonian Basin at subseasonal timescales, (ii) to analyze how these large-scale circulation patterns relate to rainfall variability in the Amazon Basin and (iii) to infer the existing connections between the southern and northern part of the Amazonian Basin in terms of regional circulation/rainfall patterns. This analysis of daily rainfall variability will be conducted thanks to long-term time series of in situ daily rainfall data collected in Bolivia and northern Brazil.

This study is organised as follows. Section 2 describes the atmospheric and rainfall data used in this paper. The clustering approach chosen to define circulation patterns based on Self-Organizing Maps (SOM; Kohonen 2001) is detailed in Sect. 3, as well as the methodology to relate large-scale circulation patterns (CPs) and rainfall. Then, an exhaustive description of the fall austral season CPs characterizing the Amazon Basin is provided in Sect. 4, with an emphasis on their temporal evolution and relationship with rainfall in southwestern and northwestern regions of the Amazon Basin where in situ daily data are available. Comparisons are also made with the CPs of other seasons, which are detailed in the Appendix. Summary and final remarks are presented in the last section of this paper.

2 Data description and pre-processing

2.1 Observed rainfall data

Daily rainfall observations have been collected in two subregions of the Amazon Basin over the period from 1975 to

2002 at locations indicated in Fig. 1c: 17 rainfall stations in the Southwest (upper Madeira basin in the Bolivian plain) and 23 rainfall stations in the Northwest (Solimões and Rio Negro basins in the northwestern Brazil). Data in Bolivia have been provided by the Bolivian National Service of the Meteorology and Hydrology (SENAMHI) while data in Brazil have been provided by the Brazilian National Water Agency (ANA).

The choice of the selected sub-regions has first been driven by the availability of daily data. These two regions indeed display the largest number of daily rainfall data over long periods. These regions have also been selected because they display contrasted rainfall and discharge variability at interannual (Espinoza et al. 2009a, 2009b), seasonal (Fig. 2) and intra-seasonal timescale, with frequent extreme daily values in the South and a more uniform distribution in the Northwest (Fig. 2c).

The homogeneity of rainfall data between rainfall stations has first been checked on interannual timescales using the Regional Vector Method (Brunet-Moret 1979) over the Amazon Basin (Espinoza et al. 2009a). At daily time steps, the coherence between nearby rainfall stations has been investigated (Mestre 2000) and the stations or periods that disagree with the nearby stations have been removed. After this quality control, rainfall stations used in this work have however less than 10% of missing values.

The spatial mean daily rainfall has been calculated for both sub-regions using a Thiessen Polygon method (Thiessen 1911). In these two regions, extreme precipitations have been defined for each season as days where rainfall exceeds the 0.90 percentile for each of the sub-regions.

2.2 Reanalysis ERA–40

The description of atmospheric circulation in the region and its subseasonal variability is based on daily values of the 40-yr European Centre for Medium-Range Weather Forecast (ECMWF) Re-Analysis (ERA–40, Uppala et al. 2005). ERA-40 data are available on a 2.5 × 2.5° grid (http://data-portal.ecmwf.int/data/d/era40_daily). As this study aims at describing the subseasonal variability in this region, low frequencies, as seasonal and interannual timescale variability, are eliminated by cutting off frequencies larger than 60-day using a high-pass Hanning filter (e.g. Leloup et al. 2008; You-Soon et al. 2004). Each season has then been analysed separately to account for the seasonal particularities of the atmospheric circulation in this region.

The clustering used to define large-scale circulation patterns (CPs) is conducted on ERA-40 850 hPa zonal and meridional winds at each grid point in the region between 10°N and 30°S and 50°W and 80°W thus 17 × 13 = 221 grid points with two variables leading to a 442 dimensional system. The 850 hPa winds are highly relevant to describe the atmospheric circulation patterns in South American tropics. These low level winds allow a proper description of the variability of the trade winds, the Northwest winds at the East of the Andes, the Low Level Jet and the southern winds. The latter features both drive water vapour advection and convergence that strongly constrain rainfall occurrence in this region. Adding other levels and/or variables (such as temperature, geopotential height, etc.) in the clustering algorithm gives similar CPs and do not change the overall quality of the rainfall discrimination. The region over which the clustering is performed has been optimally selected to discriminate at best the rainfall variability over the Amazonian Basin. Selecting a domain considerably larger (e.g. entire South America) or smaller (e.g. only southern or northern part of the basin) results in a less accurate discrimination of precipitation in the two sub-regions where in situ data are analyzed. However, slightly changing the boundaries of the domain (±5°) do not

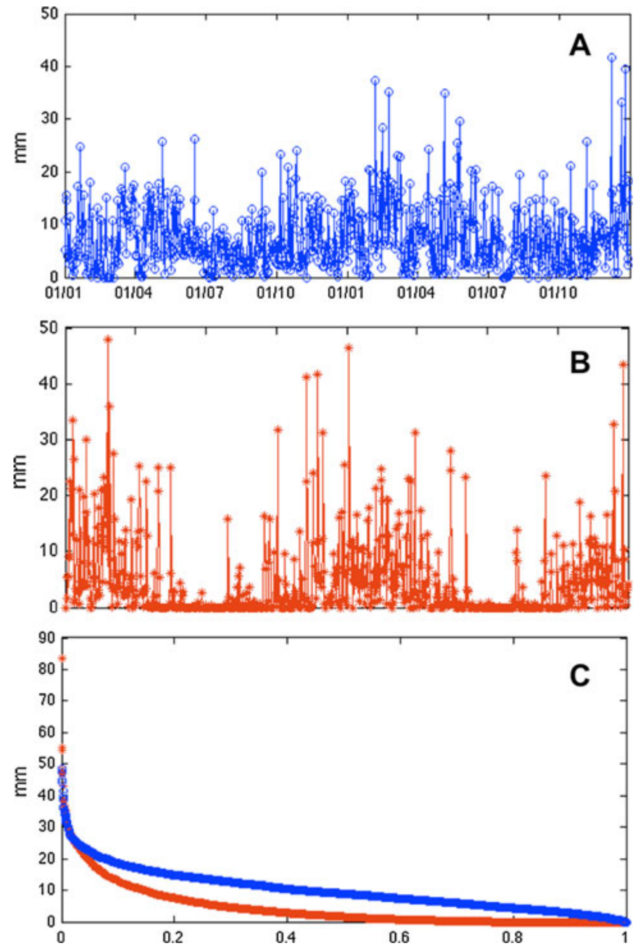

Fig. 2 **a** Mean daily rainfall in 1980 and 1981 for (**a**) the Northwest of the Amazon Basin (*blue box* in Fig. 1c) and **b** the South of the Amazon Basin (*Red box* in Fig. 1c). **c** Probability Density Function for MAM rainfall (1975–2002 period). *Blue and red lines* are for mean rainfall values in the Northwest and the South of the Amazon Basin, respectively

significantly changes the results presented in Sect. 4. In addition to the low level winds used in the CPs definition, we will also discuss winds divergence and 850 hPa geopotential height variability, but these variables do not enter the definition of the CPs. Before applying the SOM and the clustering, a normalisation is applied so that the low level winds time series is divided by its corresponding standard deviation at each grid point. This allows giving similar weight to each points of the selected region in the clustering algorithm and hence prevents giving too much weight to the southern part of the basin where the variability is known to be stronger (Marengo et al. 2004; Zipser et al. 2004).

2.3 The NOAA outgoing longwave radiation data

The daily interpolated Outgoing Longwave Radiation (OLR) data from NCAR/NOAA (Liebmann and Smith 1996) are also used over the period of study as a proxy for deep convection (e.g. Lau and Chan 1986; Liebmann et al. 1999; Jones et al. 2004). The analysis of this additional data set allows checking the robustness of our results with in situ and ERA-40 rainfall data and documenting rainfall variability in regions where in situ data were not available.

3 Defining large-scale circulation patterns in the Amazon Basin

To define large-scale circulation patterns (CPs), we use a Self-Organizing Maps (SOM), a neuronal network method, combined with a Hierarchical Ascendant Classification (HAC; Jain and Dubes 1988) to cluster the daily meteorological situations into a reduced number of CPs. CPs are then related to daily rainfall in the Amazon Basin. A similar methodology has been used by Gueye et al. (2010), which have demonstrated its efficiency in defining CPs over West Africa and relating them to rainfall over Senegal.

3.1 Clustering patterns of large-scale atmospheric variability using self-organising maps (SOM)

The clustering of the low level winds is conducted in this study by using the SOM method (Kohonen 1984, 2001). It is an unsupervised clustering algorithm which can be used for data reduction. Recent studies have shown the pertinence of this method in climatology sciences. Niang et al. (2003) use SOM to find the optics proprieties of the aerosols, analysing the ocean colour with images from satellites. This method also allowed characterizing the spatial structure of the ENSO phenomena in the observations (Leloup et al. 2007) and the IPCC-AR4 data set (Leloup et al. 2008). For similar purposes as in this study, this clustering method has also been used to define the main synoptic circulation patterns relevant for understanding rainfall variability in Pennsylvania (Hewitson and Crane 2002), in the North of Mexico and Texas (Cavazos 1999) and during the summer monsoon season over Senegal (Gueye et al. 2010).

In this study, a daily meteorological situation is composed of a two components vector (filtered zonal and meridional components of the 850 hPa wind) defined onto a 17×13 grid points of a geographical map. The set of daily meteorological situations for the 23 seasons (1979–2001) is denoted the learning set. The SOM algorithm builds a non-linear projection of the learning set onto a two-dimensional array of neurons, called Kohonen map (here a 7×7 array). This method allows summarizing the information contained in this learning set by producing a small number of reference vectors that are statistically representative of the learning set. Each reference vector represents a meteorological situation (a two components wind vector defined on the 17×13 geographical map) having statistical characteristics similar to those of the learning set. The 49 (7×7) reference vectors represent the learning set by compressing the information embedded in it. Each neuron of the Kohonen map is then defined by a reference vector, summarizing the meteorological situations contained in a subset of the learning set sharing common statistical properties, and its position on the Kohonen map. Each neuron is connected to adjacent neurons by a neighbourhood relationship.

The SOM is an iterative algorithm. Technical aspects of the algorithm can be found in Richardson et al. (2003). Further details about the procedure followed in this study are described in Leloup et al. (2007, 2008). Briefly, after initialisation, all daily meteorological situations are associated at each step to their best representative reference vector according to the Euclidian distance. Each reference vector is then updated as the weighted average of its associated daily meteorological situations, according to an adjustment coefficient. Neighbouring referent vectors are also updated to a less degree depending on a neighbourhood Gaussian function. The training stops when the reference vectors converge to a stabilized map. After this training, each daily meteorological situation is finally associated to one of the 49 reference vectors and a group of similar daily atmospheric situations associated to the same reference vector forms a cluster. Then, each final reference vector summarizes a particular pattern of variability and is representative of this cluster. On the map, nearby neurons (and associated reference vectors) correspond to similar patterns. The dimension of the output map depends on the complexity of the studied problem and upon the level of detail desired in the analysis. In this work, Kohonen map has been tested using several maps with dimensions varying from 5 × 5 to 10 × 10 neurons, without changing the characteristics of the defined CPs nor the quality of the rainfall discrimination. Results are displayed in the following for an intermediate 7 × 7 Kohonen map (i.e. 49 neurons).

Details about the SOM and its advantages with regards to other classification methods such as the k-means can be found in Badran et al. (2004). Shortly, the SOM algorithm is a generalization of k-means, allowing a more refined clustering especially when the data set may be partitioned in form of an erratic cluster set. This is due to the fact that the SOM algorithm uses in the cluster determination specific terms that take into account the topology of the cluster map, through some distance between the associated cluster neighbourhoods. Then SOM allows preserving topological relations, i.e. patterns that are close in the input space will be mapped to units that are close in the output space, and vice versa, then enabling easy visualization. Moreover, SOM is less sensitive to the initialization choices and is less prone to local optima than k-means. The search space is better explored by SOM, due to the effect of the neighbourhood parameter which forces units to move according to each other in the early stages of the process. The end result is that the neurons on the grid become ordered: neighbouring neurons have similar referent vectors. On the other hand k-means gradient orientation can force a premature convergence which, depending on the initialization, may yield local optimum solutions.

Figure 3 illustrates the results after applying this SOM algorithm to the 2116 daily meteorological situations gathered in the 23 March–April–May (MAM) seasons over the 1979–2001 period. Figure 3a displays the number of daily meteorological situations projected on each neuron for a map computed using 850 hPa winds, for the MAM season. The daily atmospheric situations described by the reference vectors corresponding to nine selected neurons (located at the extremities of the Kohonen map, indicated in Fig. 3a) are displayed in Fig. 3b. The 850 hPa wind field divergence, calculated from the wind field displayed on the neurons, is not used in the entry vector but its projection on the map allows highlighting the relationship between the atmospheric variability and rainfall events. The top part of the map clusters days displaying northern winds anomalies East of the Andes and convergence on the Bolivian plain and on the northern La Plata Basin. In contrast, the low part of the map clusters days displaying southeastern winds anomalies with divergence (convergence) appearing on the South (Northwest) of the Amazon Basin. On the centre and low right corner of the Kohonen map, the anti-clock wise rotation of the winds indicates a reinforcement of the South Atlantic Anticyclone. In contrast, the South Atlantic Anticyclone is weak on the centre and top left corner of the Kohonen map. This preliminary analysis therefore reveals that SOM is able to capture a large diversity of large-scale atmospheric situations in the entry data set. It displays a clear topological order, with opposite well defined atmospheric situations in upper and lower part of the map, while the centre of the map describes a variety of transition phases.

The daily atmospheric conditions associated with the rainiest days in both sub-regions defined in Sect. 2.1 can then be identified on the Kohonen map (Fig. 3c). This processing allows identifying the large-scale circulation patterns (CPs) associated to strongest rainfall. Rainfall and atmospheric patterns relationship will be described in detail in part 3.3.

3.2 Defining large-scale circulation patterns using Hierarchical Agglomerative Clustering

The large number of subsets provided by the SOM map allows accounting for the complexity of the dataset while conserving their relation of similarity. To further synthesize this information, we aggregate the 49 neurons into a smaller number of clusters based on the similarities of the reference vectors using a Hierarchical Agglomerative Clustering (HAC, Jain and Dubes 1988) algorithm. The HAC computes a hierarchical clustering of the 49 reference vectors of the Kohonen map according to the Ward criterion (Ward 1963), based on Euclidean distance. This criterion ensures that one will find, at each step, a local minimum of the intra-class inertia (sum of the inertia of the different clusters). The HAC aims at obtaining a classification such that each reference vector belonging to a cluster is as close as possible to the other reference vectors of this cluster, and as far as possible from the reference vectors belonging to any other cluster. The final number of cluster is selected choosing the most significant discriminative partition with respect to the dendrogram of the HAC (Fig. 4a). In this dendrogram, each leaf of the tree is a subset of neurons, each node of the tree represents the conjunction of two clusters, the size of its branches being representative of the distance between two clusters. This dendogram allows identifying the statistical optimum number of classes, the level in the dendrogram where there is a significant change of the aggregation index, based on the intra-classes variance using the Ward distance metric. For instance, in MAM, the neurons have been classified in 7 classes, because the last important difference in dissimilarity observed between nodes occurs between nodes 6 and 7 in the dendrogram. These 7 classes that aggregate days displaying similar large-scale low level circulation, are defined as the 7 CPs for MAM season (Fig. 4b).

The combination of SOM and HAC takes benefit of the respective advantages of these two algorithms. A suitable

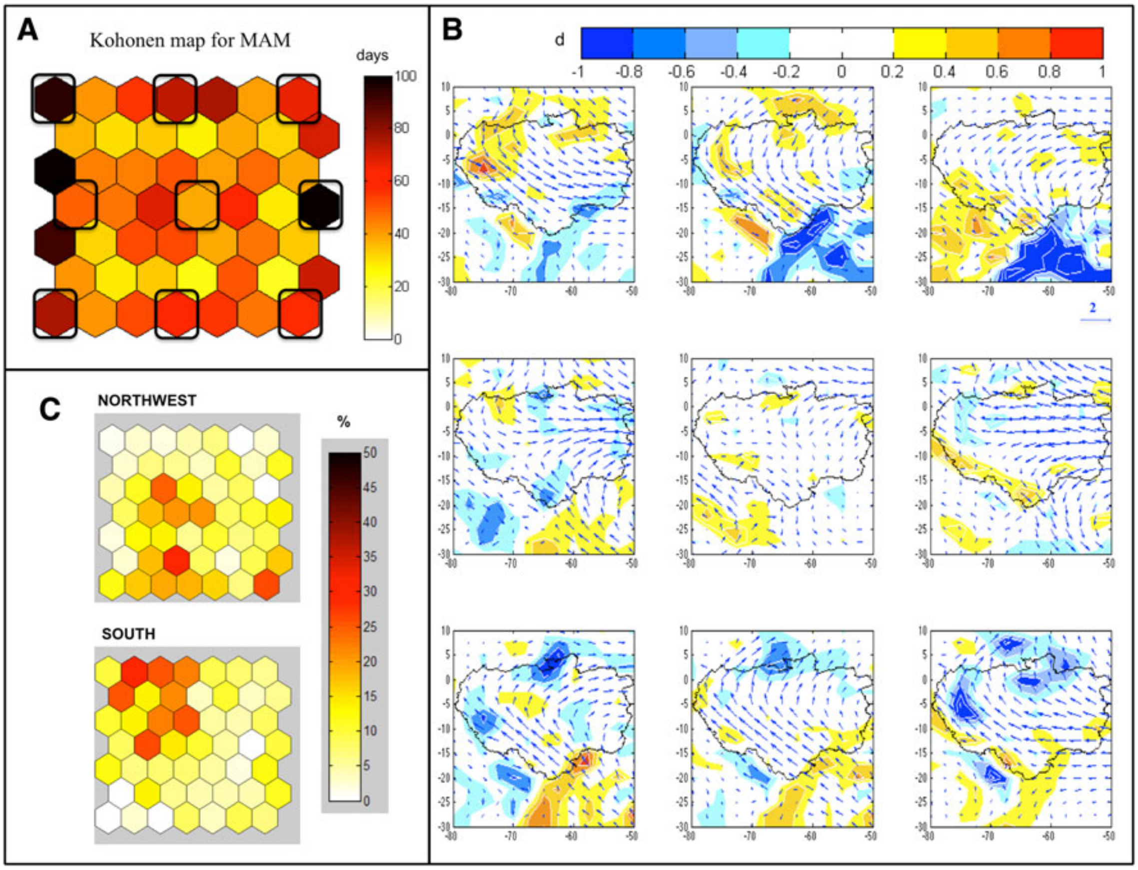

Fig. 3 **a** Kohonen map computed with subseasonal zonal and meridional winds at 850 hPa for MAM season over the 1975–2002 period in the region 10°N–30°S; 50°W–80°W. The total numbers of days projected on the Kohonen map are indicated in the *vertical scale*. **b** Subseasonal winds (*arrows*) and divergence (*color*) anomalies at 850 hPa representative of nine neurons highlighted in *panel A* (the values are normalized at each grid-point by their standard deviation). Limits of the Amazon Basin are indicated. **c** Percentage of rainy days projected onto each neuron in the Northwest (*top*) and South (*bottom*) of the Amazon Basin projected on the Kohonen map

statistical test allows to easily define the number of classes with HAC, except when the number of data in the learning set is too high. On the other hand SOM can easily interpret a high number of data. This approach hence enables to cope with the issue of defining the initial classes number, which is critical with k-means-like algorithms. As SOM is less sensitive to this choice, we can define a high number of neurons at the initialization of the SOM algorithm, and then apply the HAC to select a reduced number of classes.

The transition probability between CPs and the persistence of each CP have also been computed to capture the CPs temporal evolution (Fig. 5a) by associating each day to their corresponding CP, which allows obtaining a vector that represents the temporal sequence of CPs. The transition measures the probability for a CP to be followed by another CP. Persistence measures the probability for a CP to persist from 1 day to another. To evaluate the transition and persistence significance probability, the vector that associates each day to CPs has been reproduced randomly 1000 times (preserving the same number of days for each CP). Only significant transition values are drawn in Fig. 5a; they represent around 70% of the total possible connections between CPs. They show that specific transitions characterize the temporal evolution of the CPs. Figure 5b shows the mean low level winds related to each CP in MAM season, as well as 850 hPa divergence that allows to relate the atmospheric variability with rainfall events.

3.3 Large-scale circulation patterns and south–northwest rainfall relationship in the Amazon Basin

The precipitation index (I_k) displayed in Eq. 1 allows quantifying the relationship between CPs and rainfall in both regions of the Amazon Basin.

$$I_K = \left(\frac{P_{JK}/J_K}{J_{PT}/J_T} - \frac{J_{PT}}{J_T} \right) \times 100 \qquad (1)$$

where P_{JK} is the number of rainy days in the CP K; J_K is the total number of days projected on the CP K; J_{PT} is the total number of rainy days in the Kohonen map and J_T is total

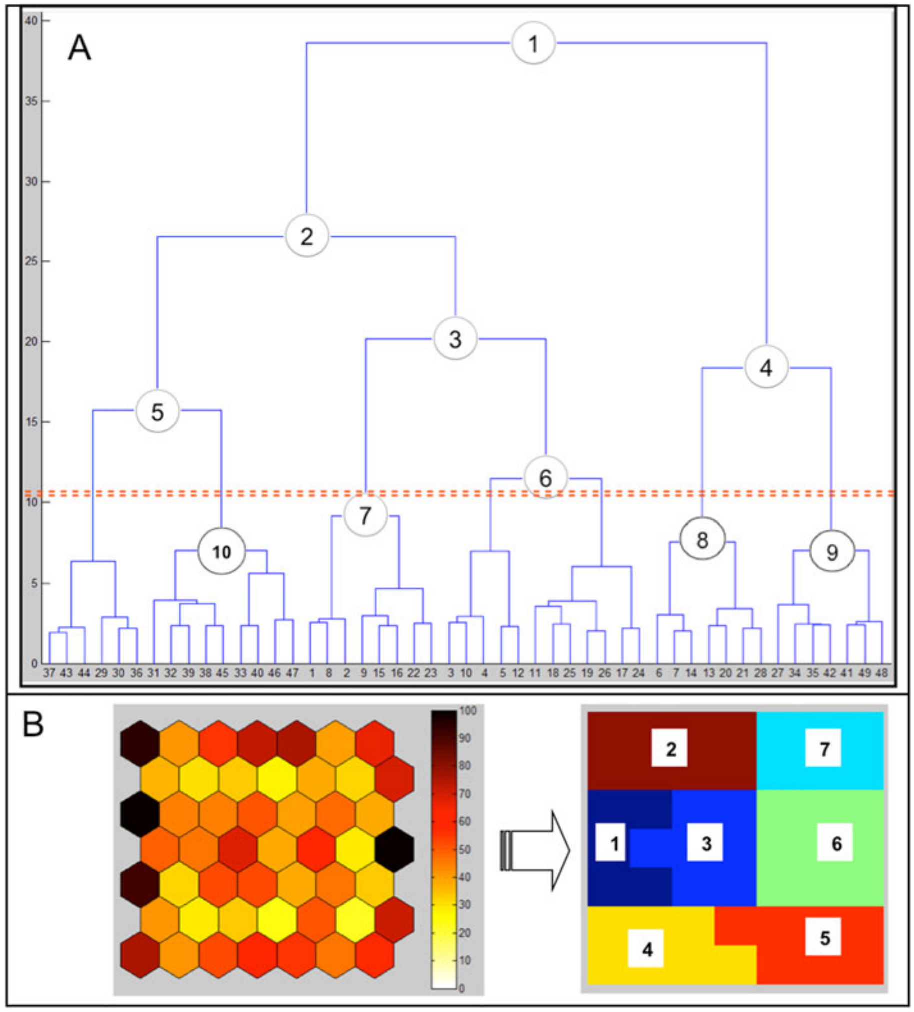

Fig. 4 **a** Dissimilarity tree resulting from AHC applied on reference vectors of the Kohonen map, for MAM season. The nodes of the dissimilarity tree are indicates with numbers from 1 to 10. **b** Classification of 49 reference vectors (*left*) into 7 CPs (*right*) according to the truncation of the dissimilarity tree indicated with a *dashed red line* in **a**

number of days on the map (Fig. 5c). Zero I_k value indicates that the percentage of rainy days projected on the CP do not differ from the mean percentage of rainy days during the season. I_k indicates the capacity of the CPs to discriminate rainy days (strong and positive I_k) and dry days (strong and negative I_k). I_k values between 25 and 25% are not represented in the figures.

Two additional analyses complement the daily precipitation variability inferred from this in situ index for both southern and northwestern Amazonian Basin: for each CPs, OLR anomalies (Fig. 6b) which can be used to relate convective activity with rainfall events and ERA40 precipitation (Fig. 7b) are displayed over the all Amazonian to check the robustness of our results and document rainfall variability in regions where in situ data were not available.

Positive I_k values characterize CP 2 and CP 3 in the southern region (white triangles pointing toward top); both CPs show strong convergence (Fig. 5b), high negative OLR anomalies (Fig. 6b) and positive ERA40 precipitation anomalies (Fig. 7b) in the Bolivian plain. Other CPs show weak or negative I_k values for the South (no triangle or white triangles pointing toward bottom in Fig. 7a, c). The northwestern region exhibits strong I_k values for CP 4 and 5 (black triangles pointing toward top) that do display convergence, strong convective activity and precipitations in ERA40 dataset in the northern Amazon Basin (Figs. 5b, 6b, 7b respectively). Strong and negative I_k values are computed for CPs 7 and 2 (black triangles pointing toward down); these CPs are associated with divergence in the Northwest of the Amazon Basin (Fig. 5b). In conclusion, rainfall in the Northwest projects principally on the lower left part of the Kohonen map, while rainfall in the South projects predominately on the top left corner of the map. Finally, Figs. 3, 5 and 6 demonstrate that this methodology does show some skill in discriminating rainy and dry days in both Northwest and South of the Amazon Basin simultaneously.

To compare ERA40 precipitation to in situ data, ERA-40 I_k values are also displayed on Fig. 7c. In general, I_k

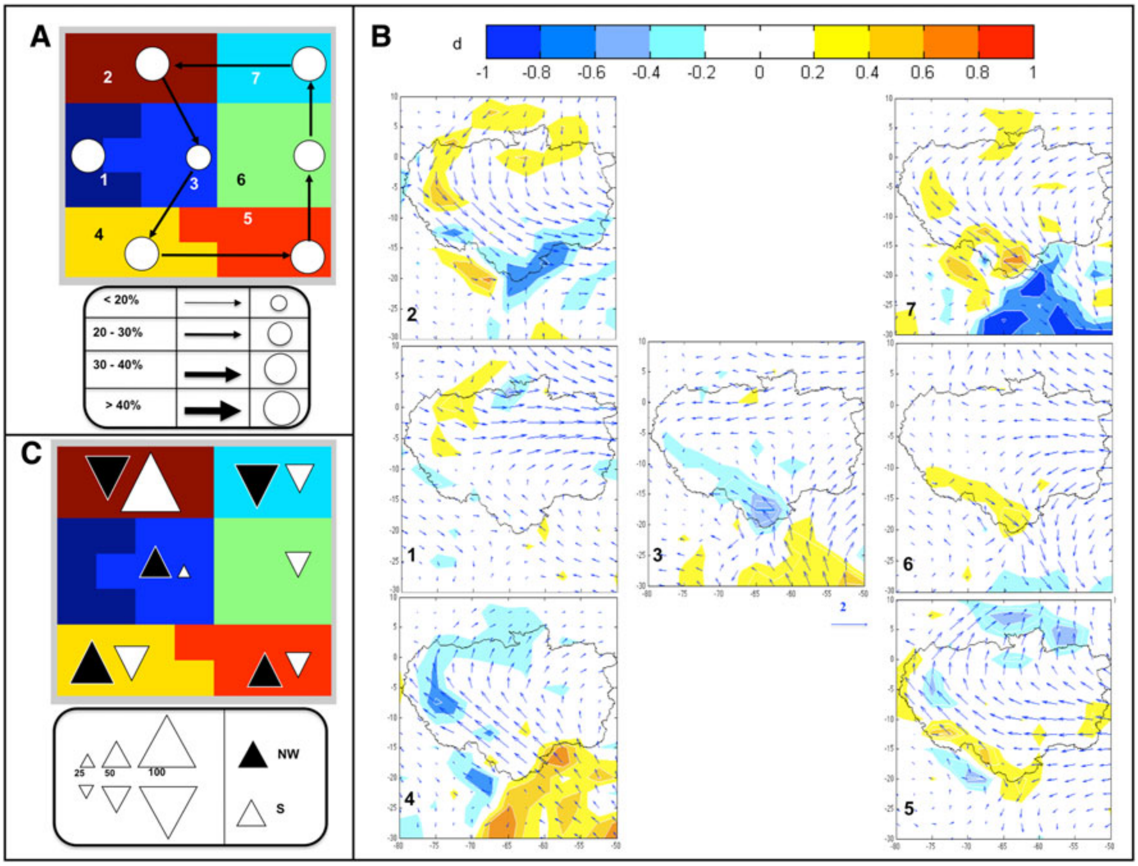

Fig. 5 **a** Delimitation of the 7 CPs defined on the Kohonen map for MAM (*color*) and probabilities of persistence (*white circles*) and transition (*black arrows*), in percentage. **b** Subseasonal winds (vector) and divergence (color) anomalies at 850 hPa normalized at each grid-point by their standard deviation associated with each CP. The limit of the Amazon Basin is plotted. **c** I_k values (in %) for each CP for the Northwest (*black triangles*) and the South (*white triangles*) of the Amazon Basin. Positive (negative) I_k values are represented using upward (downward) triangles

values from ERA-40 and observed data do show similar tendencies in the South of the basin. Nevertheless differences can be observed in the I_k magnitudes, i.e. CP 3, CP 5 and CP 6. In the Northwest of the Amazon Basin, important differences are noticed. Coherence between observed and ERA-40 I_k values are only found in CP 2 and CP 4, when the rainfall anomalies are the strongest in this region.

4 Description of the large-scale circulation patterns in the Amazon Basin

Although CPs are defined from low level winds in the 10°N–30°S; 50°–80°W region, 850 hPa winds and geopotential anomalies for each CP have been displayed in Fig. 8b over a larger region (i.e., 15°N–60°S and 0°–120°W) to document the continental atmospheric circulation related to each CP.

In between seasons, several CPs display similarities, but some specific CPs are seasonal. The most important differences have been observed in DJF season, while during MAM, JJA and SON seasons, CPs are similar, particularly for the CPs sequence from CP 2 to CP 7.

In Sect. 4.1, CPs sequences from CP 2 to CP 7 are described for MAM season (Figs. 5, 6, 7, 8). CPs for DJF season and seasonal CPs characteristics are described in Sect. 4.2. CPs for JJA and SON seasons are available in the Appendix.

4.1 Sequence of large-scale circulation patterns for March–April–May season

For MAM season, the temporal evolution between the different CPs shows a clear tendency to describe a cycle from CP2 to CP7, with southern wind anomalies and their convergence with the trade winds progressing northward from the La Plata Basin to the Amazon Basin. A detailed description of these CPs and their temporal evolution is provided in the following.

CP 2 gathers meteorological situations associated with negative geopotential height anomalies and western to northwestern winds anomalies over the Amazon Basin

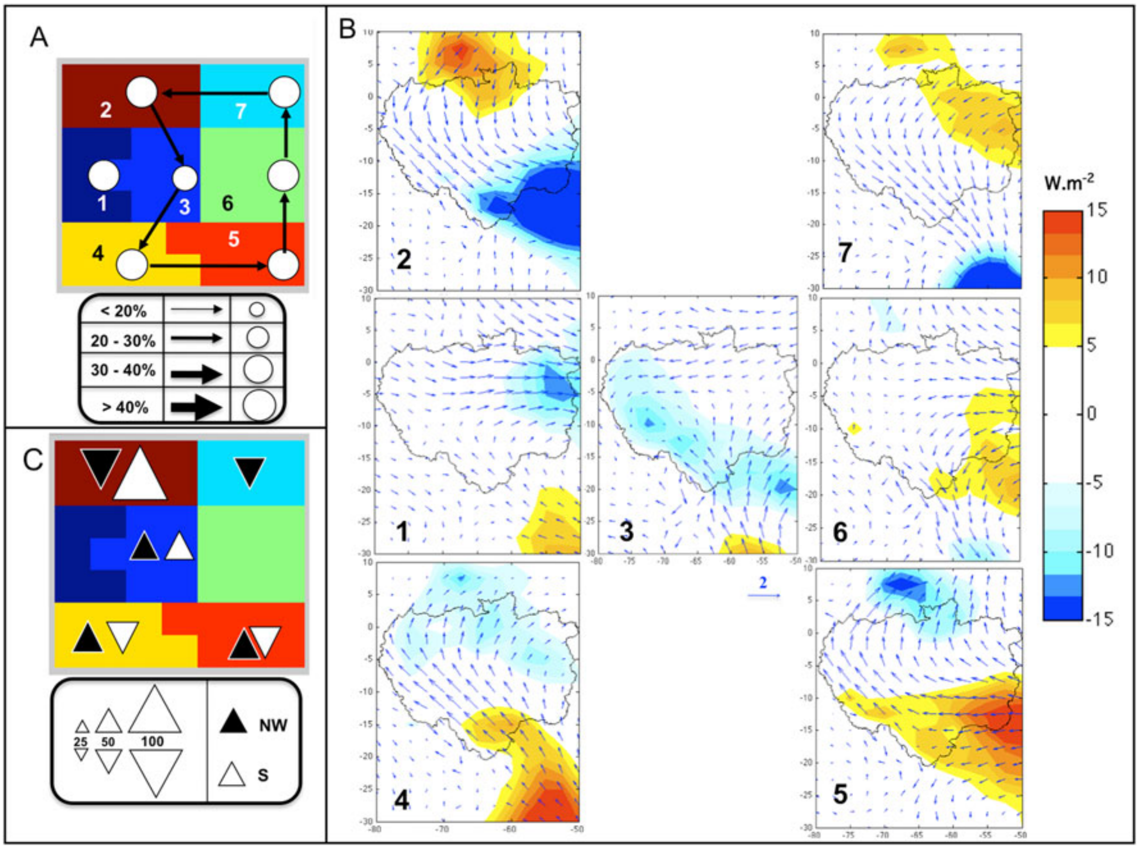

Fig. 6 As Fig. 5 but plotting OLR anomalies from NCAR/NOAA onto each CP in MAM. OLR anomalies less (greater) than –5 (5) W.m^{-2} are plotted. Figure 5c shows I_k values computed using OLR instead rainfall data

(Fig. 8b). The weaker than usual South Atlantic Anticyclone and negative geopotential height anomalies over southeastern South America results in southern winds anomalies south of the Amazon Basin that converge with northern winds anomalies at the East of the Andes. These low level winds patterns explain the convergence, convective activity and rainfall found in the southern Amazon Basin and divergence and dry conditions in its northwestern part (Figs. 5, 6, 7). ERA-40 and OLR datasets further reveals that convergence, convection and positive rainfall anomalies are evidenced in central-East Brazil (Figs. 6b, 7b, 8b). These conditions are characteristic features of cold front advection (Garreaud and Wallace 1998), of the negative phase of the SACZ when the convergence is stationary (Nogues-Peagle and Mo 1997; Carvalho et al. 2002a; Liebmann et al. 2004) and of western (Jones and Carvalho 2002; Carvalho et al. 2002b) and northern wind regimes (Wang and Fu 2002). CP 2 appears in 16% of the total MAM days and its persistence is high (52% of the cases—Table 1 and Fig. 5, respectively).

From CP 2 to CP 3, the aforementioned geopotential height anomalies are displaced eastward and the geopotential height over the Chaco strengthens (Fig. 8b). This results in southern winds anomalies in the southern Amazon Basin (as far as 5–10°S). Consequently, convergence, convection and rainfall are displaced northward forming an elongated stripe from southern to Northwest Amazon, resulting in rainfall events in both selected regions (Figs. 5, 6, 7). CP 3 has a central location in the map. This is consistent with its transient characteristics between northern (CP 2) and southern (CP 4) winds anomalies on one hand, and eastern and western regimes on another hand. It is also noticeable that this transient CP has a weak persistence (34%; Fig. 5a). Southern winds anomalies observed during CP 2 and CP 3 in Argentina and South of the Amazon Basin, respectively, are very similar to the results obtained by Garreaud and Wallace (1998).

For CP 4, the positive geopotential height anomaly over the Chaco low further increases and spread all over the continent (Fig. 8b). As a consequence, the southern winds anomalies east of the Andes are displaced further north and intensify (Figs. 5b, 8b). The consecutive weakening of the northwestern winds at the east of the Andes is related to extra-tropical eastward propagating perturbations developing over the two adjoining oceans, with a negative geopotential height anomaly in the South Pacific

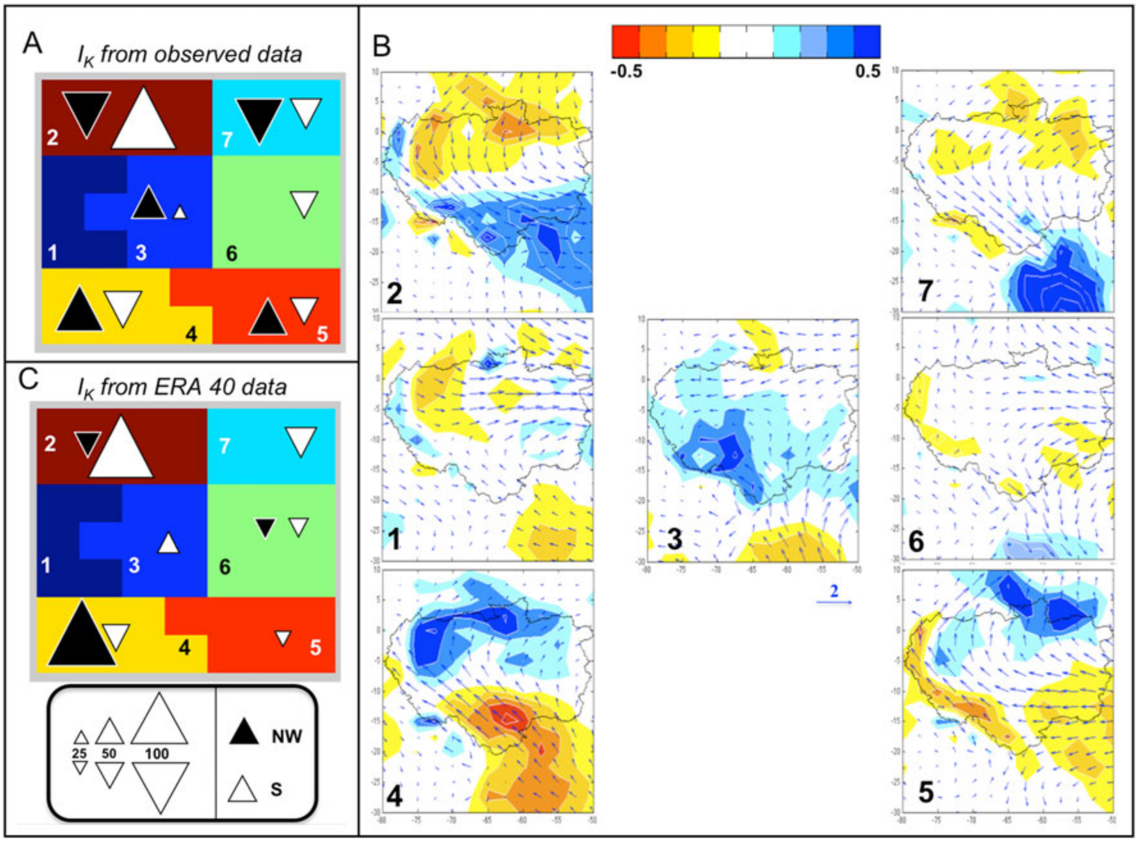

Fig. 7 **a** As Fig. 5c. **b** As Fig. 5b, but plotting rainfall from ERA-40 onto each CP in MAM (the values are normalized at each grid-point by their standard deviation). **c** As Fig. 5c, but I_k values are computed using rainfall data from ERA-40

Anticyclone region, a positive one on the continent and another negative one in the South Atlantic Anticyclone region (Fig. 8b). This pattern is typical of westerly wave propagation in the southern hemisphere, with the strongest signature at 500 hPa, but also detected at 850 hPa (Kiladis and Weickmann 1992; Ambrizzi and Hoskins 1997). Strong divergence, weak convection and negative rainfall anomalies occur in the South of the Amazon Basin as well as the North of the La Plata Basin, while rainfall is displaced toward the northwest of the Amazon Basin featuring a no-SACZ situation (Figs. 5b, 6b, 7b). ERA-40 and OLR data show that rainfall is also observed in the whole northern Amazon, associated with convergence and strong convection (Figs. 5b, 6b, 7b). 13% of the total MAM days are characterized by CP 4, which persists in 50% of the cases (Table 1 and Fig. 5a, respectively).

Positive subtropical geopotential anomaly then progresses eastward toward the Atlantic Ocean (Fig. 8b). Consequently, during CP 5 easterly winds anomalies take place in the South of the Amazon Basin. These anomalies then are deviated northward when approaching the Andes (Figs. 5b, 7b, 8b). As for CP 4, they generate convergence and rainfall in the northwest and the north and divergence in the south featuring a no-SACZ episode, but in this case, convection activity is stronger in the northern hemisphere (Fig. 6b). CP 5 wind and OLR anomalies are very similar to those displayed during easterlies (Fig. 5 in Carvalho et al. 2002b) and cross-equatorial southerly regimes (Wang and Fu 2002). CP 5 occurs during 13% of the total MAM days and it is persistent in 54% of the cases (Table 1 and Fig. 5a, respectively). From CP 2 to CP 5 the anomalous southern winds experience a large meridional excursion, from 50 to 5°S, as documented by Garreaud and Wallace (1998). These authors also mention that southern winds move at a mean speed of 10 m/s and retain their identities over intervals of about 5 days.

During CP 6, positive geopotential height anomaly shifts further east while weakening. A negative geopotential height anomaly develops on the southern tip of the continent, highlighting the beginning of a new Chaco low episode (Fig. 8b). Consequently, divergence and dry conditions persist in the south of the Amazon Basin as during CP 5 but convection begins to develop in the La Plata Basin (Figs. 5b, 6b, 7b). This CP corresponds to the ending of the easterly regime, to a southern position of a cold front and characterizes the positive phase of the SACZ, (Nogues-Peagle and Mo 1997 and Liebmann et al. 2004). CP 6 is the most frequent circulation pattern as it

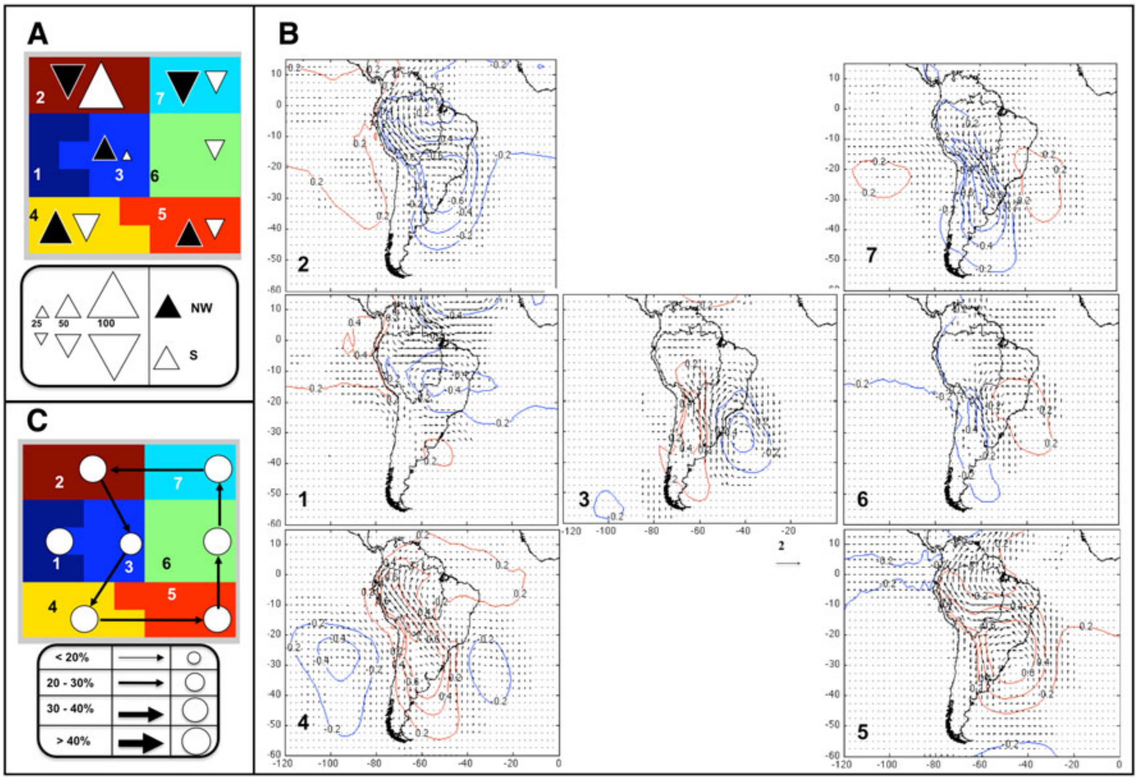

Fig. 8 **a** As Fig. 5c, **b** Subseasonal winds and geopotential height anomalies at 850 hPa associated with each CP for the 15°N–60°S and 0–120°W region, in MAM (only normalized wind anomalies higher than 0.2 are drawn). *Red and bleu lines* correspond to positive and negative of geopotential height, respectively, normalized at each grid-point by their standard deviation. Limits of South America and Amazon Basin are plotted. **c** As Fig. 5a

is observed during 18% of the MAM days and it is persistent in 34% of the cases (Table 1 and Fig. 5a, respectively).

During CP 7, the Chaco low further strengthens and extends northward. A succession between positive geopotential high in South Pacific Anticyclone, negative geopotential height anomaly on the Chaco and a positive in South Atlantic Anticyclone also characterizes CP 7. This CP is the CP 4 anti-phase (Fig. 8b) and corresponds to the development of a westerly and cross-equatorial northerly regime and to a cold front located over northern Argentina. Those conditions results in a strong northern winds anomaly (LLJ included), which transports humidity from Amazon Basin toward La Plata Basin. During CP 7 divergence and negative rainfall anomalies appear in the whole Amazon Basin and positive OLR anomalies show up in the eastern part of the basin, indicating an absence of convection in this region (Figs. 5b, 6b, 7b). At ERA-40 and OLR data, strong convection and rainfall are also evidenced in the north of the La Plata Basin as a consequence of humidity transfer from the Amazon Basin (Marengo et al. 2004). 13% of the total MAM days are characterized by CP 7, which is persistent in 46% of the cases (Table 1 and Fig. 5a, respectively).

The most probable evolution is a northeastward progression of the negative geopotential height anomaly and the set up of CP 2, which ends the circuit of the temporal organization of the CPs (Fig. 5a), with a recurrence of a westerly regime. Transition from CP 7 to CP 2 is very similar to the atmospheric conditions described in Mendes et al. (2007), during day 0 and day +1 of a cyclogenesis event in South America. On average, the cycle described from CP 2 to CP 7 is completed in about 10 days.

CP 1 is characterized by weak, negative and unstructured geopotential height anomalies (shallow low) over the Amazon Basin (Fig. 8b), weak trade winds and no rainfall anomaly (Fig. 5b). Figures 6b and 7b show that no rainfall and convective anomaly are observed in the South and a slight negative rainfall anomaly appears in the Northwest of the Amazon Basin. Moreover strong and negative OLR anomalies are dominant in the eastern part of the basin, indicating an important convective activity in this region during CP 1. None of the trajectories observed from or to CP 1 are statistically significant. Consequently, CP 1 in Fig. 5a appears isolated of the temporal organization of the CPs.

These results demonstrate that our method is able to capture large-scale atmospheric features associated to

Table 1 Characteristics of the CPs during each season: frequency of CPs (days in %), mean rainfall associated with CPs in the Northwest (R-NW) and the South (R-S), frequency of dry days by season (R-NW = 0 and R-S = 0) and maximal rainfalls in each CP by region (Max NW and Max S)

Season	CP	Days (%)	R-NW (mm)	R-S (mm)	R-NW = 0 (%)	R-S = 0 (%)	Max NW	Max S
MAM	1	13	**8.6**	4.8	0.6	23.8	33.9	38.6
	2	16	**7.5**	**7.4**	0.5	5.9	35.0	83.7
	3	14	**12.0**	**6.2**	0.0	13.0	47.2	55.1
	4	13	**12.1**	**2.3**	0.3	50.2	48.5	26.0
	5	13	**11.2**	**3.3**	0.3	33.0	44.1	28.9
	6	18	10.0	**3.4**	0.0	23.4	34.8	43.2
	7	13	**8.9**	**3.4**	0.3	21.2	24.6	25.2
JJA	1	12	7.0	**0.3**	1.0	76.8	23.4	21.4
	2	17	**6.5**	**1.5**	1.7	51.4	30.7	26.0
	3	16	**7.6**	**2.1**	0.3	47.1	35.0	37.0
	4	13	**8.6**	**0.4**	1.2	77.3	39.6	34.0
	5	10	**6.9**	**0.2**	2.0	85.9	24.3	6.3
	6	16	**6.9**	**0.2**	2.5	89.9	26.2	22.4
	7	16	7.3	**0.5**	0.2	74.7	29.9	33.1
SON	1	9	**8.2**	**3.3**	0.0	30.8	31.2	44.5
	2	16	**5.4**	**6.8**	1.6	14.7	27.7	42.7
	3	18	**7.5**	**8.1**	0.9	12.3	39.1	58.2
	4	7	**9.8**	**3.4**	0.6	38.4	40.0	41.1
	5	13	7.2	**1.9**	1.5	61.4	26.2	37.9
	6	10	**6.2**	**2.7**	1.6	39.2	36.0	24.1
	7	13	**5.2**	**2.8**	2.3	35.7	27.0	29.5
	8	15	7.1	**3.1**	0.6	31.1	25.7	52.1
DJF	1	21	**8.3**	**7.2**	0.8	5.8	33.2	43.2
	2	9	**5.7**	**10.3**	5.9	7.7	26.0	73.0
	3	11	**9.7**	**8.0**	0.7	4.0	49.4	54.1
	4	24	**11.1**	**6.3**	0.0	7.3	39.6	33.3
	5	15	**9.7**	7.1	0.0	10.9	41.7	42.2
	6	18	**7.3**	**9.0**	3.8	2.4	41.6	65.5

Rainfalls values in bold are different from mean rainfall according to Student test

SACZ and LLJ variations, extra-tropical perturbations and related convective events in both southern and northern Amazon Basin. However, no specific CPs are dedicated to describe the detailed atmospheric circulation that occurs during smaller scale and shorter lived events such as instability lines propagating from the Atlantic Ocean toward the Amazon Basin or mesoscale convective complexes in the southern part of the basin. This is likely to be related to our choice to compute CPs from daily atmospheric reanalysis data while the typical life cycle of a squall line lasts about 17 h (Satyamurty et al. 1998). We however performed an additional analysis reavealing that squall lines events described by Cohen et al. (1995) occur during specific large-scale conditions: when identifying the circulation patterns corresponding to the days described as squall line 2 events (SL2) in Cohen et al. (1995) between 04/13/1987 and 05/13/1987 (Table 1 in Cohen et al. 1995), it appears that 72% of SL2 cases are related to CPs 4 and 5 (easterly regimes), that are indeed related to rainfall events in the north of the Amazon Basin. Focusing on the period from May the 5th to May the 8th 1987 (also investigated in details in Cohen et al. 1995) reveals that the circulation on May 5th is associated with CP 4 while the other days (May 6th, 7th, 8th) corresponds to CP 5. This case study analysis therefore suggests that the large-scale conditions described by CP 4 and 5, which are also related to easterly regimes, might favour SL2 events.

4.2 Specific large-scale circulation patterns during December–January–February season

During DJF season, 6 CPs are defined using the methodology described in part 3.1 and 3.2. Throughout this season, CPs are less spatially and temporally organized than during other seasons (i.e. in terms of transition probabilities and low level winds spatial structures) and they are more persistent than in other seasons (Fig. 9). The evolution from one CP to another does not describe a well-defined sequence, as it was the case for MAM. However, CPs 1, 2 and 5 show very similar atmospheric patterns compared to the corresponding CPs for MAM season while most of the others CPs described in the following do resemble, to some extent, to one of the CPs described for MAM.

CP 6 in DJF, a variant of CP 2, shows a negative anomaly of the geopotential height in the northwest of the La Plata Basin, which promotes northern winds anomalies in the whole Amazon Basin associated to monsoon flux, and southern winds advection from La Plata Basin toward the Bolivian plain (Fig. 9b). Consequently, convergence and a positive rainfall anomalies are observed in the South of the Amazon Basin, while a negative I_k value is observed in the Northwest of the Amazon Basin, similarly to CP 2. During DJF, CP 6 and CP 2 occur frequently (27% vs. 16% in others seasons, Table 1); this is consistent with a greater activity of the SACZ during summertime (Kodama 1992; Liebmann et al. 1999; Carvalho et al. 2004).

The more probable trajectory from CP 6 is toward CP 3 (Fig. 9c), characterized by an unstructured atmospheric pattern (or “shallow high” as CP 1 during MAM), with slight positive geopotential height and stronger than usual trade winds on the Amazon Basin; it is an anti-phase of MAM and DJF CP 1 (Figs. 8b, 9b). During DJF, CP 1 and CP 3 represent 32% of the days (Table 1), which is exceptional in relation with others seasons. This is coherent with the fact that DJF is the warmest season, with the smallest frequency of extra-topical perturbations, which are weaker and confined to the south. The more probable transition of CP 3 is toward CP 6 (Fig. 9c).

CP 4 during DJF shows a similar pattern than CP 5 in MAM, but the negative geopotential anomaly is centred further north and the wave is not so clearly organized (Fig. 9b). As described for CP 5 and CP 4 in MAM, rainfall conditions oppose the Northwest and the South of the Amazon Basin (positive and negative I_k values, respectively). The more probable transition is toward CP 3 and CP 5 (Fig. 9b).

CP 4 and CP 7 in MAM are not observed in DJF. These CPs with large meridional winds anomalies featuring important mass air exchanges between tropics at the east of

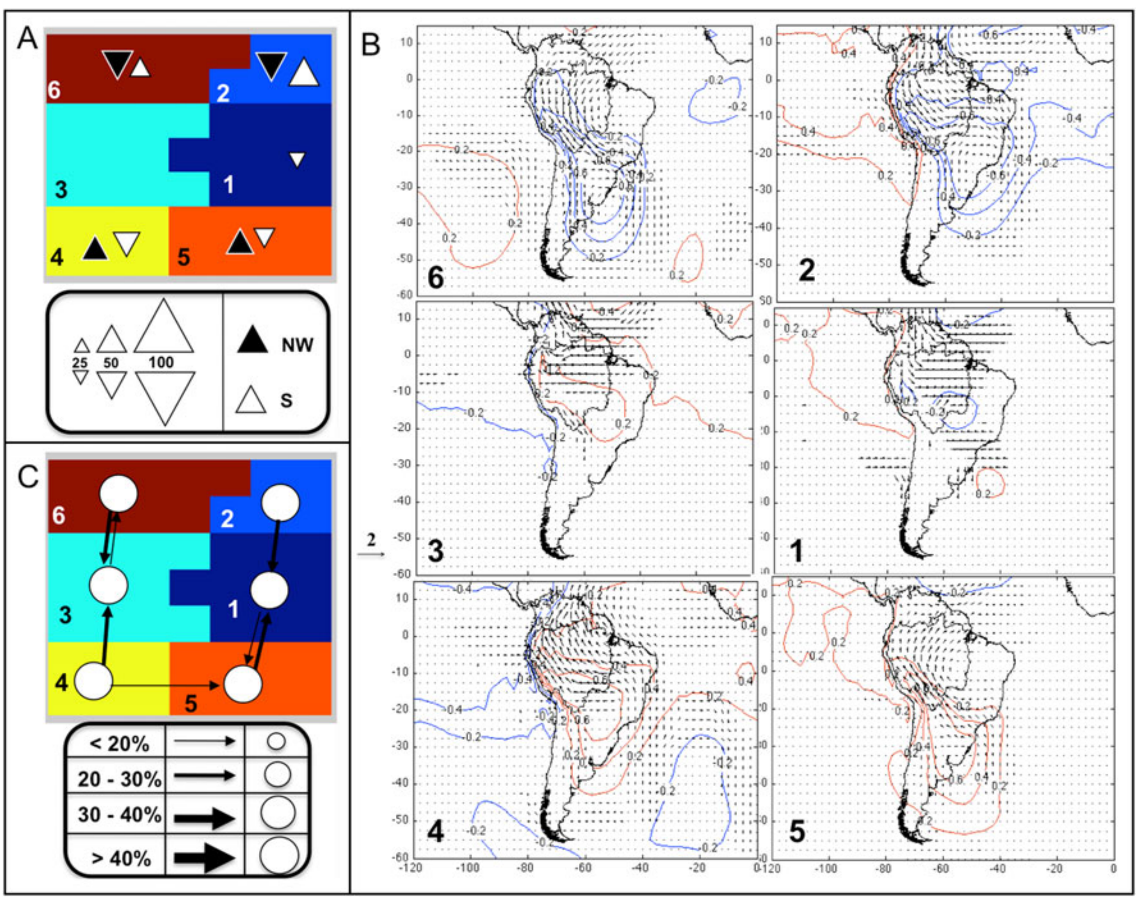

Fig. 9 As Fig. 8, but for December–January–February season. Here 6 CPs have been defined using the procedure described in Sects. 3.1 and 3.2

the Andes and extratropics are characteristics of colder seasons, when the latitudinal temperature gradient is pronounced and originates strong perturbations.

4.3 Circulation patterns statistics

For MAM and JJA seasons, days are equally distributed over each CPs, while some CPs do gather considerably more days than others for SON and DJF (Table 1). As expected, mean rainfall associated to CPs are coherent with the corresponding I_k values.

Table 1 further reveals contrasted rainfall statistics between the northwest and the South of the Amazon Basin. In the Northwest, rainfall differences between CPs are weaker than in the South. For instance, in JJA, rainfall varies between 6.5 mm/day (CP 2) and 8.6 mm/day (CP 4) in the Northwest and between 0,2 (CP 5 and CP 6) and 2.1 mm/day (CP 3) in the South. The rainfall ratio is 1 for 10 in the South while much smaller in the Northwest. Furthermore, in the Northwest, days with no rainfall events are very rare (of the order of 1%) while they are more common in the South, varying, for instance, from 51,4% (CP 2) to 89.9% (CP 6) during JJA season. Thus, during the warm season, rainfall differences between CPs are of the same order in the Northwest and in the South and the percentages of days with no rain are generally smaller than 10% in both regions. This result corroborates the stronger seasonality in the South compared to the Northwest of the Amazon Basin, a well known feature already discussed in several previous studies (i.e. Figueroa and Nobre 1990; Espinoza et al. 2009a).

In accordance with the stronger convection in the South (Zipser et al. 2006; Durkee et al. 2009), maximum rainfall values associated with each CP (MAX-SW in Table 1) highlight that the largest daily rainfall during the 1975–2002 period have been observed in the South where they exceed 50 mm/day various times. For instance, during DJF season, the maximum rainfall value is 73 mm/day (CP 2) in the South, while it is 49 mm/day (CP 3) in the Northwest. However, during the dry JJA season the maximum rainfall values are quite similar in both regions (see Fig. 2a, c).

Different characteristics of the CPs confirm that the methodology applied in this work is able to identify large-scale atmospheric patterns at subseasonal timescale explaining rainfall in two regions with very different features in seasonality and rainfall frequency distributions (Fig. 2).

5 Summary and final remarks

This study describes and analyses the main large-scale atmospheric circulation patterns (CPs) in the Amazonian Basin over the 1975–2002 period. The CPs are defined by means of a method based on Self-Organizing Maps or Kohonen Maps and Hierarchical Agglomerative Clustering applied to daily 850 hPa winds of ERA-40 Reanalysis. Daily satellite Outgoing Longwave Radiation (a proxy for deep convection) and ERA-40 precipitation data over the whole domain as well as in situ rainfall data in both the northwestern and southern regions of the Amazon Basin allowed investigating the relationship between these large-scale atmospheric patterns and rainfall variability. This study is an attempt to provide a synthetic description of the large-scale atmospheric patterns existing over the Amazon Basin at subseasonal timescales and to relate them with regional rainfall variability. It complements former studies that were dedicated to pluviometic events in the tropics or subtropics and to particular atmospheric features as SACZ, LLJ, extra-tropical perturbations (e.g. Nogues-Peagle and Mo 1997; Carvalho et al. 2002b; Marengo et al. 2004; Oliveira and Nobre 1986; Garreaud and Wallace 1998). Here, the low level wind and rainfall variability are analyzed in order to understand how these two variables are associated at intraseasonal timescale and how convergence, convection and rainfall evolve within space and time. Although the chosen methodology based on a large domain size (the all Amazonian Basin) and a daily temporal resolution does not allow to specifically capture small scale and short lived atmospheric events such as instability lines, our approach recognises the main large-scale fluctuations affecting South American climate associated with SACZ, LLJ and mid-latitude waves variability and allows describing the existing connections between the southern and the northern part of the Amazon Basin.

The identified CPs display a well-organized temporal evolution describing a 6 to 8 phases cycle lasting about 10 days. CPs organisation and evolution are strongly associated with eastward moving extra tropical perturbations and their incursion toward low latitude that modulate geopotential and winds over South America and its adjoining oceans. These CPs are shown to be related to rainfall anomalies in the southern and northern part of Amazon Basin. Figure 10 synthesizes the four main atmospheric conditions explaining extremes rainfall in this region.

The first main circulation pattern is characterized by northern winds anomalies North of 20°S, resulting from a southward deflection by the Andes of the reinforced trade winds, convergence with southern winds anomalies at higher latitudes, hence producing heavy convection and rainfall in the La Plata Basin (Fig. 10a). These convective events have also been noticed during regimes of westerly (Carvalho et al. 2002b) and northerly inds (Wang and Fu 2002), the positive phase of the SACZ (Nogues-Peagle and Mo 1997) and the passage of cold fronts all around the year (Marengo et al. 2004). This pattern is related to a negative geopotential anomaly centred on the continent and positive ones over the adjoining oceans, typical of an eastward moving mid-latitude wave train. The eastward progression of this extra-tropical wave is then related with the development of a positive geopotential anomaly in the South Pacific (Fig. 10b). On its oriental flank, it drives the former southern winds anomaly towards north. Consequently, convergence of southern and northern winds anomalies, convection and extreme rainfall are displaced northward in the South of the Amazon Basin. The westerly and the northerly regimes persist, cold fronts migrate northward (as described by Garreaud and Wallace 1998) and a negative phase of the SACZ may be observed in summer. While the wave moves further East (Fig. 10c), the positive geopotential anomaly settles over the South American continent and negative geopotential anomalies develop over the adjoining oceans. The southern winds anomalies on the oriental flank of the positive geopotential anomaly converge with the trade winds in the Northwest of the Amazon Basin, providing convection and rainfall in this region. These conditions correspond to the beginning of easterly and southerly regimes (as describe by Carvalho et al. 2002b and Wang and Fu 2002, respectively) and to a no-SACZ episode (in summer), with convection limited to the north. Finally, accordingly to the eastward displacement of the wave, the positive geopotential anomaly moves over the eastern part of South America resulting in anomalous southerlies on its western flank (Fig. 10d), allowing the persistence of easterly and southerly regimes and of a no-SACZ episode in summer. This anomaly converges with the northern trade winds over Northeastern Amazon providing rainfall in this region.

This CPs analysis has been conducted separately for each season but our results indicate that CPs, and related rainfall, are rather similar through the year. Nevertheless, during DJF season the spatio-temporal organization of the CPs is somehow different, mostly due to weaker extra tropical waves and more frequent shallow low situations, with very weak rainfall anomalies.

Finally, the simultaneous use of daily OLR, in situ and ERA-40 rainfall data allows confirming the existing relationships between CPs and rainfall anomalies over the Amazon Basin. Our results reveals that precipitation variability is better reproduced by ERA-40 in the southern part of the Amazonian Basin than the northern part, where rainfall variability is likely to be more constrained by local and subdaily processes (e.g. squall lines) that could be misrepresented in the reanalysis dataset. A dedicated study at subdaily frequencies would be necessary to investigate the atmospheric conditions related to instability lines, that propagate from the mouth of the Amazon river into the Amazon region. The lack of observed rainfall data over a long period in this region and an accurate representation of these phenomena in reanalysis could however prevent for the moment to thoroughly investigate the relationship between the atmospheric and rainfall variability at these time-scales.

This work demonstrates the potential of using CP to better understand local rainfall variability in the Amazon Basin. Particularly, it supplies important information about large-scale atmospheric circulation and extreme rainfall relationship in the northern part of the Amazon, as well as interactions between southern and northern rainfall. Indeed,

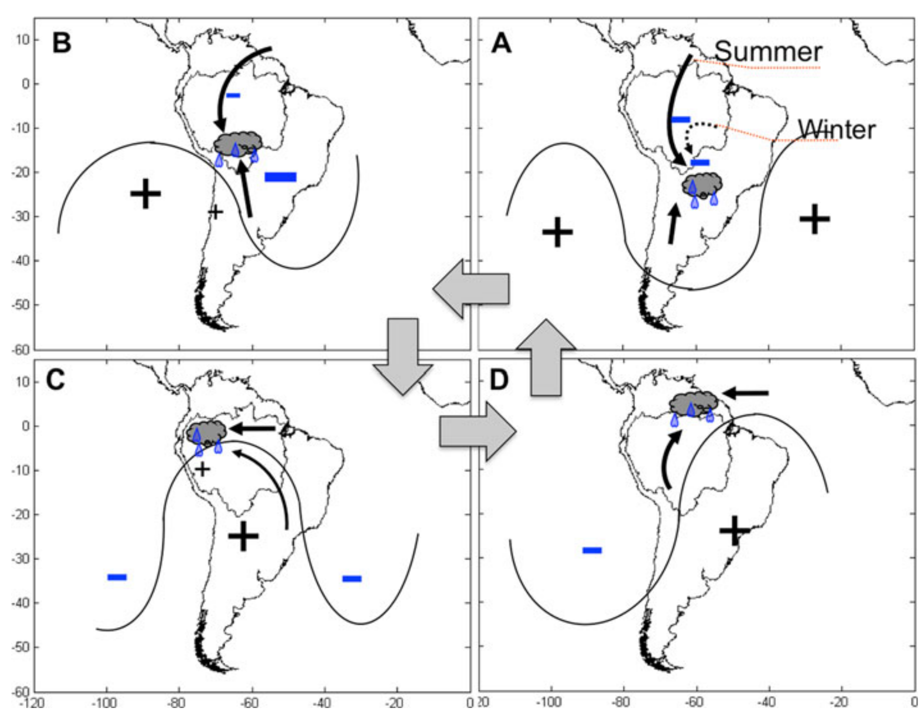

Fig. 10 Simplified schema of the atmospheric circulation at 850 hPa associated with rainfall in **b** the South and **c** the Northwest of the Amazon Basin. "+" and "−" symbols correspond to positive and negative geopotential height anomalies, respectively, and *arrows* represent winds anomalies

former studies mainly focused on strong rainfall events in tropical and subtropical South America (Carvalho et al. 2002a, 2004, for instance), disregarding dry events in these regions (that are also rainy spells in northern Amazon). Though, these dry episodes, if long-lasting, may also be of interest for economical and agricultural purposes in the South.

The ability of CPs to explain part of the rainfall variability is encouraging, and taking advantage of the relationships between rainfall and river discharge, the relationship between extreme hydrological events and the frequency of occurrence of some specific CPs is now under investigation (Espinoza 2009). Moreover, this method could also be very useful to characterize the evolution of these CPs in a warmer climate. Inferring how these CPs and related rainfall are likely to evolve in the context of climate change is also of great socio-economical concern for South-America. The IPCC AR4 (Intergovernmental Panel on Climate Change Fourth Assessment Report) coupled ocean–atmosphere simulations are good candidates for such an investigation. We are currently performing a thorough assessment of the ability of these models to reproduce the observed CPs and their relation to rainfall for present climate using a similar methodology before investigating their possible evolutions in the future.

Acknowledgments The authors would like to express their special thanks to the Institute of Research for the Development (IRD), the French National Center for Scientific Research (CNRS) through the REGYNA (Rainfall regionalisation and hydrological and agronomical impacts of climate change in vulnerable regions) program and the European CLARIS-LPB (European South American network for Climate Change Assessment and Impacts Studies) program for funding this research. ECMWF ERA-40 data used in this study has been provided by ECMWF from the ECMWF data server. We especially thank Gérard Cochonneau and Philippe Vauchel, the SENAMHI (Servicio Nacional de Meteorología e Hidrología—Bolivia) and ANA (Agência Nacional de Águas—Brazil), all members of the Observatory for Environmental Research HYBAM (Hydrogeodynamics of the Amazon Basin), for providing rainfall data. Our special thanks are for our colleagues from the LOCEAN, Benjamin Sultan, Pascal Terray, Abdou Gueye, and Mathieu Vrac from LSCE, for the productive discussions about circulation Patterns determination and downscalling. Also, we are appreciative to Henning Rust for the helpful proofreading of this manuscript. Finally, we are grateful to the reviewers whose comments and suggestions considerably helped to improve this paper.

Appendix: specific large-scale circulation patterns during JJA and SON seasons

During JJA and SON, CPs are very similar to MAM (described in part 4.1). Nevertheless some CPs are

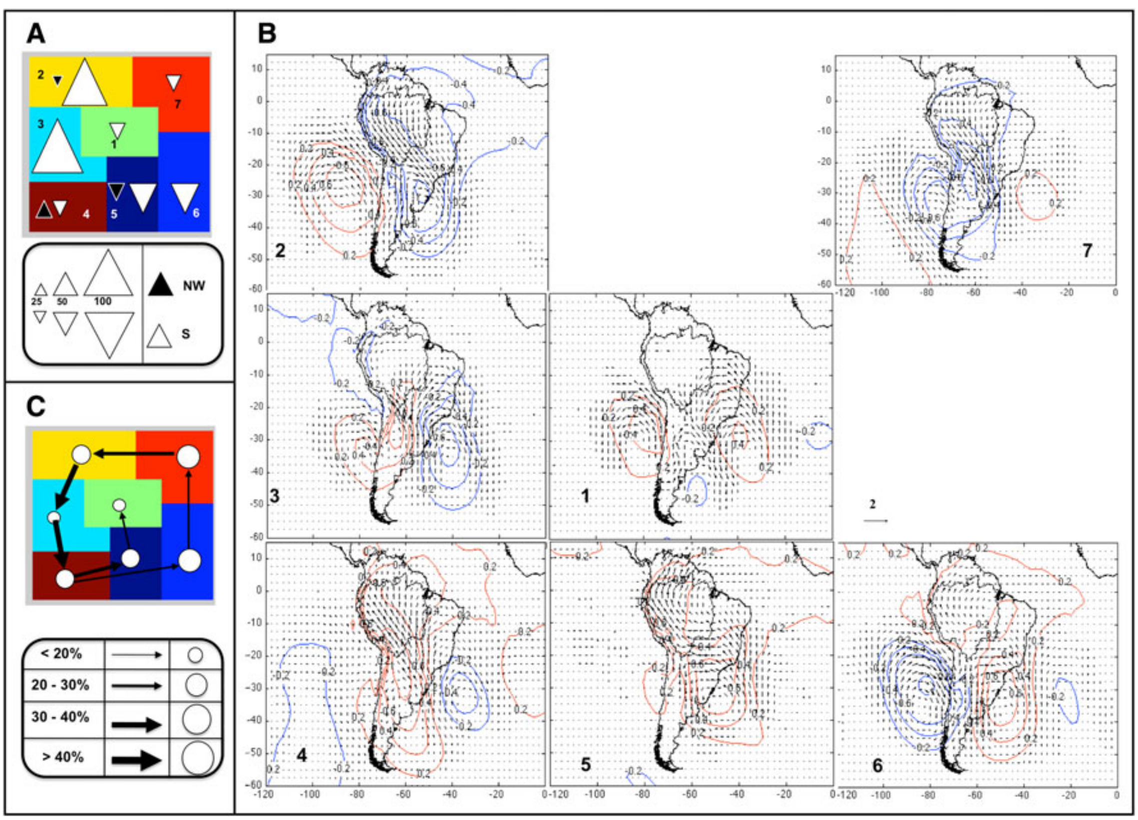

Fig. 11 As Fig. 9, but for June–July–August season

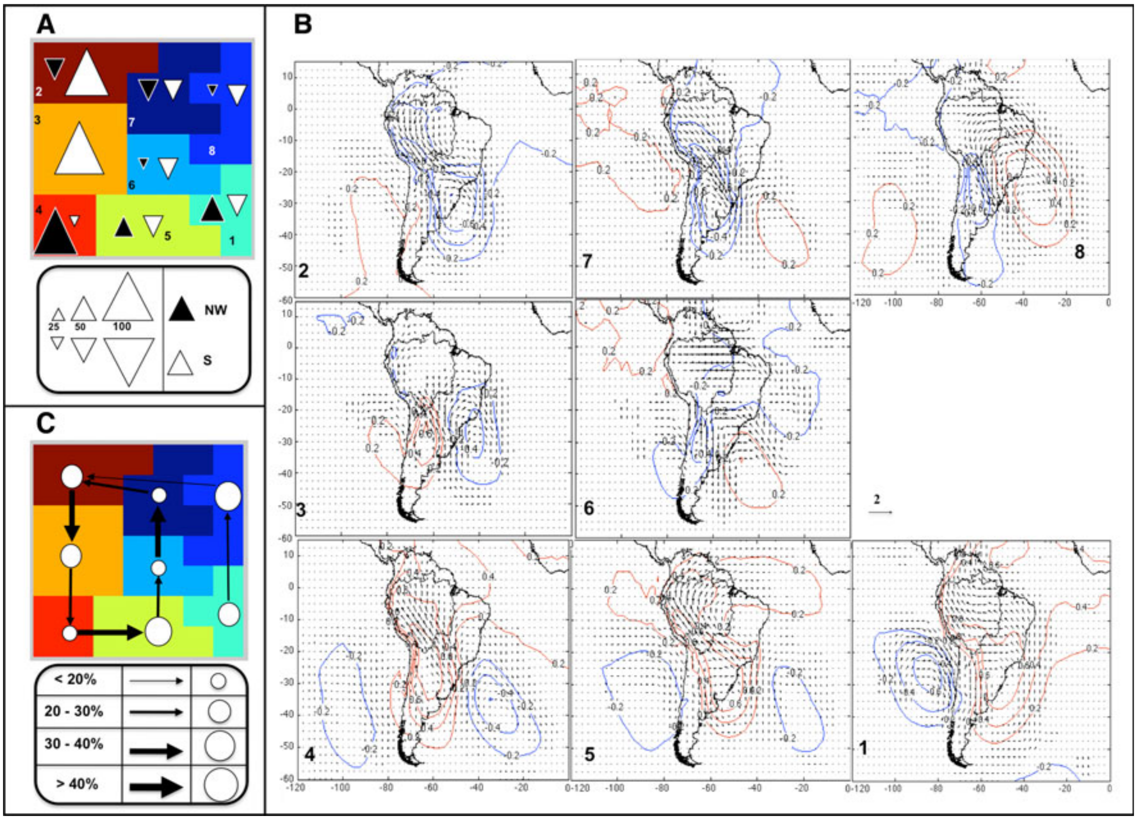

Fig. 12 As Fig. 9, but for September–October–November season. Here, 8 CPs have been defined using the procedure described in Sects. 3.1 and 3.2

particular to each season, as CP 1 during JJA and CP 1 and 8 during SON (Figs. 11, 12, respectively).

CP 1 during JJA corresponds to a transition between CP 5 and CP 7 with northwestern winds anomalies on La Plata Basin originated by a strong South Atlantic anticyclone (Fig. 11). CP 1 during JJA is also characterized by a strong South Pacific anticyclone and very slight winds anomalies in the whole Amazon Basin. Consequently, no rainfall anomaly is observed in the Northwest and a slight negative rainfall anomaly characterizes the South of the Amazon Basin (Fig. 11a). More, the weak persistence of CP 1 and CP 3 (transition CPs, in the centre of the Kohonen map) is consistent with better-structured patterns of circulation in winter.

CP 1 and 8 during SON are alternative ways, taking the place of CP 5 and CP 7 in the temporal organization of the CPs, to connect CP 4 and CP 2 (Fig. 12). CP 1 (8) is the variant of CP 5 (7). Both CP 1 and CP 8 show similar I_k values than CPs 5 and 7, respectively (Fig. 12a).

References

Ambrizzi T, Hoskins B (1997) Stationary Rossby-wave propagation in a baroclinic atmosphere. Q J R Meteorol Soc 123:919–928

Badran F, Yacoub M, Thiria S (2004) Self-organizing maps and unsupervised classification. In: Dreyfus G (ed) Neural networks: methodology and applications. Springer, Berlin

Berri GJ, Inzunza BJ (1993) The effect of the low level jet on the poleward water vapor transport in the central region of South America. Atmos Environ 27A:335–341

Bettolli ML, Penalba OC, Vargas WM (2010) Synoptic weather types in the south of South America and their relationship to daily precipitation in the core production region of crops in Argentina. Aust Meteorol Oceanogr J 60:37–48

Bischoff S, Vargas W (2003) The 500 and 1000 hPa weather circulations and their relationship with some extreme climatic conditions over southern South America. Int J Climatol 23:541–556

Bonner WD (1968) Climatology of the low level jet. Mon Wea Rev 96:833–850

Brunet-Moret Y (1979) Homogénéisation des précipitations. Cahiers ORSTOM Sér Hydrol 16:3–4

Carvalho L, Jones C, Liebmann B (2002a) Extreme precipitation events in southeastern South America and large-scale convective patterns in the South Atlantic convergence zone. J Clim 15:2377–2394

Carvalho LMV, Jones C, Silva Dias MAF 2002b Intraseasonal large-scale circulations and mesoscale convective activity in tropical South America during the TRMM-LBA campaign. J Geophys Res 29. doi:10.102/2001JD000745

Carvalho L, Jones C, Liebmann B (2004) The Southern Atlantic convergence zone: intensity form persistence and relationships with intraseasonal to interannual activity and extreme rainfall. J Clim 17:88–108

Cavazos T (1999) Large-scale circulation anomalies conducive to extreme events and simulation of daily rainfall in northeastern Mexico and southeastern Texas. J Clim 12:1506–1523
Chaves RR, Cavalcanti IFA (2001) Atmospheric features associated with rainfall variability over Southern Northeast Brazil. Mon Wea Rev 129:2614–2626
Cohen JCP, Silva Diaz MAF, Nobre CA (1995) Environmental conditions associated with Amazonian squall lines: a case study. Mon Wea Rev 123:3163–3174
De Souza EB, Ambrizzi T (2006) Modulation of the intraseasonal rainfall over tropical Brazil by the Madden–Julian oscillation. Int J Clim 26:1759–1776
Diaz A, Aceituno P (2003) Atmospheric circulation anomalies during episodes of enhanced and reduced convective cloudiness over Uruguay. J Clim 16:3171–3185
Durkee JD, Mote TL, Shepherd JM (2009) The contribution of Mesoscale convective complexes to rainfall across subtropical South America. J Clim 22:4590–4605
Espinoza JC 2009 Impact de la variabilité climatique sur l'hydrologie du basin Amazonien. Université Pierre et Marie Curie, Paris–France. Ph.D. Thesis. p 203
Espinoza JC, Ronchail J, Guyot J-L, Cocheneau G, Filizola N, Lavado W, De Oliveira E, Pombosa R, Vauchel P (2009a) Spatio-temporal rainfall variability in the Amazon Basin countries (Brazil, Peru, Bolivia, Colombia and Ecuador). Int J Clim 29:1574–1594
Espinoza JC, Guyot J-L, Ronchail J, Cochonneau G, Filizola N, Fraizy P, de Oliveira E, Ordoñez JJ, Vauchel P (2009b) Contrasting regional discharge evolutions in the Amazon Basin (1974–2004). J Hydrol 375:297–311
Figueroa SN, Nobre CA (1990) Precipitation distribution over central and western tropical South America. Climanalise 6:36–40
Fink AH, Brücher T, Krüger A, Leckebusch GC, Pinto JG, Ulbrich U (2004) The 2003 European summer heatwaves and drought–synoptic diagnosis and impacts. Weather 59:209–216
Garreaud R, Wallace JM (1998) Summertime incursions of midlatitude air into subtropical and tropical South America. Mon Wea Rev 126:2713–2733
Gastang M, Massie HL Jr, Halverson J, Greco S, Scala J (1994) Amazon coastal squall lines. Part I: structure and kinematics. Mon Wea Rev 122:608–622
Greco S, Scala J, Halverson J, Massie HL Jr, Tao WK, Gastang M (1994) Amazon coastal squall lines. Part II: heat and moisture transport. Mon Wea Rev 122:624–635
Gueye AK, Janicot S, Niang A, Sawadogo S, Sultan B, Diongue-Niang A, Thiria S 2010 Weather regimes over Senegal during the summer monsoon season using self-organizing maps and hierarchical ascendant classification. Part I: synoptic time scale. Climate dynamics. doi:10.1007/s00382-010-0782-6
Hewitson B, Crane R (2002) Self-organizing maps: applications to synoptic climatology. Clim Res 26:1315–1337
Jain AK, Dubes RC (1988) Algorithms for clustering data. Prentice Hall, Englewood Cliffs
Janowiak JE, Kousky VE, Joyce RJ 2005 The diurnal cycle of precipitation determined from the CMORPH high spatial and temporal resolution global precipitation analyses. J Geophys Res Atmos 110:D23105. doi:10.1029/2005JD006156
Jones C, Carvalho LMV (2002) Active and break phases in the South American Monsoon system. J Clim 15:905–914
Jones C, Carvalho LMV, Higgins RW, Waliser DE, Schemm JKE (2004) Climatology of tropical intraseasonal convective anomalies: 1979–2002. J Clim 17:523–539
Kiladis GN, Weickmann KM (1992) Circulation anomalies associated with tropical convection during northern winter. Mon Wea Rev 120:1900–1923
Kiladis GN, Weickmann KM (1997) Horizontal structure and seasonality of largescale circulations associated with submonthly tropical convection. Mon Wea Rev 125:1997–2013
Kodama Y (1992) Large–scale common features of subtropical precipitation zones (the baiu frontal zona, the SPCZ and the SACZ. Part I: characteristic of subtropical frontal zones. J Meteor Soc Japan 70:813–836
Kohonen T (1984) Self organization and associative memory, 2nd edn. Springer-Verlag, Berlin, p 312
Kohonen T 2001 Self–organizing maps. Springer Series in Information Sciences, 3nd edn, Springer, p 30
Lau KM, Chan PH (1986) Aspects of the 40–50 day oscillation during the northern summer as inferred from outgoing longwave radiation. Mon Wea Rev 114:1354–1367
Laurent H, Machado LAT, Morales C, Durieux L 2002 Characteristics of Amazonian Mesoscale convective systems observed from satellite and radar during the WETAMC/LBA Experiment. J Geophys Res 107(D20):8054. doi:10.1029/2001JD000337
Leloup J, Lachkar Z, Boulanger JP, Thiria S (2007) Detecting decadal changes in ENSO using neural networks. Clim Dyn 28:147–162
Leloup J, Lengaigne M, Boulanger J-P (2008) Twentieth century ENSO characteristics in the IPCC database. Clim Dyn 30:277–291
Lenters J, Cook KH (1995) Comments on "on the influence of the Andes on the general circulation of the Southern hemisphere". J Clim 8:2113–2115
Liebmann B, Smith CA (1996) Description of a complete (interpolated) outgoing longwave radiation dataset. Bull Am Meteorol Soc 77:1275–1277
Liebmann B, Kiladis GN, Marengo JA, Ambrizzi T, Glick JD (1999) Submonthly convective variability over South America and the South Atlantic convergence zone. J Clim 12:1877–1891
Liebmann B, Kiladis G, Vera C, Saulo C, Carvalho L (2004) Subseasonal variations of rainfall in South America in the vicinity of the low-level jet east of the Andes and comparison to those in the South Atlantic convergence zone. J Clim 17: 3829–3842
Maddox RA (1980) Mesoscale convective complexes. Bull Amer Meteor Soc 110:1374–1387
Marengo J, Cornejo A, Satymurty P, Nobre C, Sea W (1997) Cold surges in tropical and extratropical South America: the strong event in June 1994. Mon Wea Rev 125:2759–2786
Marengo JA, Soares WR, Saulo C, Nicolini M (2004) Climatology of the low level jet east of the Andes as derived from the NCEP-NCAR reanalysis. Characteristics and temporal variability. J Clim 17:2261–2280
Mendes D, Souza EP, Trigo IF, Miranda PMA (2007) On precursors of South-American cyclogenesis. Tellus A 59:114–121
Mestre O 2000 Méthodes statistiques pour l'homogénéisation de longues séries climatiques. PhD. Tesis. Universit Paul Sabatier, Toulouse, p 229
Michelangeli PA, Vautard R, Legras B (1995) Weather regimes: recurrence and quasi stationarity. J Atmos Sci 52:1237–1256
Molinier M, Guyot JL, Oliveira E, Guimarães V (1996) Les régimes hydrologiques de l'Amazone et de ses affluents. L'hydrologie tropicale : géoscience et outil pour le développement, Paris, Mai 1995. IAHS Publ 238:209–222
Montes de Oca I (1995) Geografía y clima de Bolivia (geography and climate of Bolivia). Bull Inst Fr Etud Andines 24:357–368
Moron V, Robertson A, Ward M-N, Ndiaye O (2008) Weather types and rainfall over Senegal. Part I: observational analysis. J Clim 21:266–287
Niang A, Badran F, Moulin C, Crépon M, Thiria S (2003) Retrieval of aerosol type and optical thickness over the Mediterranean from seawifs images using an automaticneural classification method. Remote Sens Environ 100:82–94

Nogues-Peagle J, Mo K (1997) Alternating wet and dry conditions over South America during summer. Mon Wea Rev 125:279–291

Oliveira AS, Nobre CA 1986 Meridional penetration of frontal systems in South America and its relation to organized convection in the Amazon. Publication INPE-3407-PRE/676

Petersen WA, Nesbitt SW, Blakeslee RJ, Cifelli R, Hein P, Rutledge SA (2002) TRMM observations of intraseasonal variability in/over the Amazon. J Clim 15:1278–1294

Planchon O, Damato F, Dubreuil F, Gouery P (2006) A method of identifying and locating sea-breeze fronts in north-eastern Brazil by remote sensing. Meteorol Appl 113:1–10

Poveda G, Waylen P, Pulwarty R (2006) Annual and inter-annual variability of the present climate in northern South America and southern Mesoamerica. Palaeogeogr Palaeoclimatol Palaeoecol 234:3–27

Richardson AJ, Risien C, Shillington FA 2003 Using self-organizing maps to identify patterns in satellite imagery. Progress in Oceanography, vol 59. Pergamon, pp 223–239

Rickenbach TM (2004) Nocturnal cloud systems and the diurnal variation of clouds and rainfall in southwestern Amazonia. Mon Wea Rev 132:1201–1219

Ronchail J (1989) Advections Polaires en Bolivie: mise en évidence et caractérisation des effets climatiques. Hydrol Cont 4:49–56

Satyamurty P, Nobre CA, Silva Dias PL 1998 Tropics—South America. In: Karoly DJ, Vincent DG (Org.) Meteorology and hydrology of the Southern Hemisphere. Boston: Meteorology Monograph. 49:119–139

Saulo AC, Nicolini M, Chou SC (2000) Model characterization of the South American low-level flow during the 1997–1998 spring-summer season. Clim Dyn 16:867–881

Solman S, Menéndez C (2003) Weather regimes in the South American sector and neighbouring oceans during winter. Clim Dyn 21:91–104

Sugahara S, Rocha RP, Rodrigues ML 1994 Condicões atmosféricas de grande escala associadas a jato de baixos níveis na América do Sul. In: Proceedings Eighth Brazilian Congress of Meteorology, vol 2. Brazilian Meteorological Society, Belo Horizonte, pp 573–577

Thiessen AH (1911) Precipitation averages for large areas. Mon Wea Rev 39:1082–1084

Uppala SM, Kållberg PW, Simmons AJ, Andrae U, da Costa Bechtold V, Fiorino M, Gibson JK, Haseler J, Hernandez A, Kelly GA, Li X, Onogi K, Saarinen S, Sokka N, Allan RP, Andersson E, Arpe K. Balmaseda MA, Beljaars ACM, van de Berg L, Bidlot J, Bormann N, Caires S, Chevallier F, Dethof A, Dragosavac M, Fisher M, Fuentes M, Hagemann S, Hólm E, Hoskins BJ, Isaksen L, Janssen PAEM, Jenne R, McNally AP, Mahfouf JF, Morcrette JJ, Rayner NA, Saunders RW, Simon P, Sterl A, Trenberth KE, Untch A, Vasiljevic D, Viterbo P, Woollen J 2005 The ERA-40 re-analysis. Quart J R Meteorol Soc 131:2961–3012

Velasco I, Fritsch JM (1987) Mesoscale convective complexes in the Americas. J Geophys Res 92:9591–9613

Vera C, Higgins W, Amador J, Ambrizzi T, Garreaud R, Gochin D, Gutzler D, Lettenmaier D, Marengo J, Mechoso C, Nogues-Paegle J, Silva Diaz P-L, Zhang C (2006) Towards a unified view of the American Monsoon System. J Clim 19:4977–5000

Wang H, Fu R (2002) Cross-equatorial flow and seasonal cycle of precipitation over South America. J Clim 15:1591–1608

Ward JH (1963) Hierachical grouping to optimize an objective function. J Am Statist Assoc 58:236–244

Xie P, Arkin PA (1997) Global precipitation: a 17-year monthly analysis based on gauge observations, satellite estimates, and numerical model outputs. Bull Amer Meteor Soc 78:2539–2558

You-Soon C, Dongchull J, Homan L, Hui SA, Jang-Won S, Yong-Hoon Y (2004) Interannual variability and lagged correlation during strong El Niño events in the Pacific Ocean. Clim Res 27:51–58

Zipser E, Salio P, Nicolini M 2004 Mesoscale convective systems activity during SALLJEX and the relationship with SALLJ events. CLIVAR Exchanges, vol 9, no 1. International CLIVAR Project Office, United Kingdom, pp 14–18

Zipser EJ, Cecil DJ, Liu C, Nesbitt SW, Yorty DP (2006) Where are the most intense thunderstorms on earth? Bull Am Meteorol Soc 87:1057–1071